Eurographics Workshop on Visual Computing for Biology and Medicine (2016)
S. Bruckner, B. Preim, and A. Vilanova (Editors)

Aortic Dissection Maps: Comprehensive Visualization of Aortic Dissections for Risk Assessment

G. Mistelbauer[1,2], J. Schmidt[1,3], A.M. Sailer[4], K. Bäumler[4], S. Walters[4], and D. Fleischmann[4]

[1]Institute of Computer Graphics and Algorithms, TU Wien, Vienna, Austria
[2]Otto-von-Guericke University, Magdeburg, Germany
[3]AIT Austrian Institute of Technology, Austria
[4]3D and Quantitative Imaging Laboratory, Department of Radiology, Stanford University School of Medicine, CA, USA

Abstract

Aortic dissection is a life threatening condition of the aorta, characterized by separation of its wall layers into a true and false lumen. A subset of patients require immediate surgical or endovascular repair. All survivors of the acute phase need long-term surveillance with imaging to monitor chronic degeneration and dilatation of the false lumen and prevent late adverse events such as rupture, or malperfusion. We introduce four novel plots displaying features of aortic dissections known or presumed to be associated with risk of future adverse events: Aortic diameter, the blood supply (outflow) to the aortic branches from the true and false lumen, the previous treatment, and an estimate of adverse event-free probabilities in one, two and 5 years. Aortic dissection maps, the composite visualization of these plots, provide a baseline for visual comparison of the complex features and associated risk of aortic dissection. These maps may lead to more individualized monitoring and improved, patient-centric treatment planning in the future.

Categories and Subject Descriptors (according to ACM CCS): I.3.3 [Computer Graphics]: Picture/Image Generation—Display algorithms I.4.6 [Image Processing and Computer Vision]: Segmentation—Edge and feature detection I.4.7 [Image Processing and Computer Vision]: Feature Measurement—Size and shape

1. Introduction

Aortic dissection **(AD)** is an uncommon [HBF*13] but life-threatening condition of the aorta (cf. Figure 1a), the main blood vessel in all vertebrates. The underlying pathology of AD is a diseased medial layer of the aorta. The acute and clinically dramatic event of an AD is characterized by the sudden development of a so-called *primary entry tear*, a defect on the luminal side of the aorta. This allows blood to enter the abnormal aortic wall and burrow ('dissect') a new, 'false' channel within the aortic wall (cf. Figure 1b). The dissected aortic wall is of lower mechanical strength, and may rupture – typically a lethal event. When the intramural blood finds its way back into the original 'true' blood flow channel of the aorta, two separate flow channels are generated (cf. Figure 1c). Since the interior of a blood vessel is called *lumen*, the two new channels are referred to as the *true lumen* (TL) and the *false lumen* (FL).

The **diagnosis** of ADs is typically established with *computed tomography angiography* (CTA), acquired in the emergency room. CTA provides detailed anatomic information of therapeutically relevant features such as TL and FL. The *Stanford classification* [DTS*70] distinguishes between *type A aortic dissection* (AAD) and *type B aortic dissection* (BAD). AADs are characterized by the involvement of the ascending aorta (the most proximal portion of the aorta), whereas BADs do not involve the ascending aorta (cf. Figures 1d and 1e). AADs are more common than BADs [DTS*70].

The **treatment** of AADs requires urgent surgical repair, whereas BADs are traditionally treated medically with blood-pressure control, unless complications occur [HBB*10]. Medical treatment is less invasive and usually better tolerated by, especially, older patients. In the case of complications (i.e., leaking, rupture or compromised blood flow to organs [FMM08]), surgical or endovascular repair is indicated. The full anatomic spectrum of ADs is broad, however, and the associations of anatomic features with early and late outcomes are not fully understood. Several features of the aorta that may indicate certain treatment strategies have been studied in isolation, but not in aggregate. The problem is that so far, associations are not apparent by only (qualitatively) assessing imaging data. Hence, a systematic visualization of several features along the aorta can help physicians to quantitatively assess the features, and derive necessary therapeutic and prognostic implications.

All survivors of ADs – including patients who underwent successful surgical or endovascular treatment, as well as those who responded well to medical management alone – require life-long surveillance with imaging to monitor the diameter of the dissected aorta. Despite medical blood-pressure control, many patients, up

DOI: 10.2312/vcbm.20161282

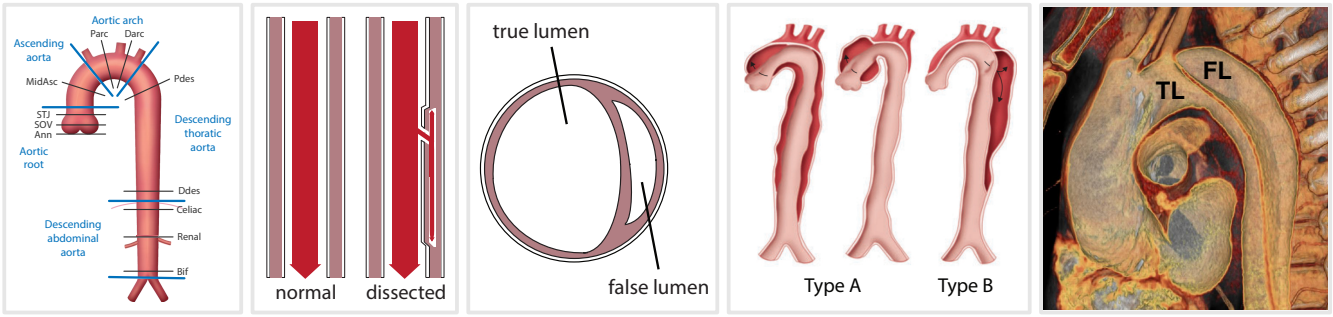

(a) Aorta layout (b) Aortic dissection (c) Dissected cross-section (d) Stanford classification (e) Example

Figure 1: *Aortic Dissection. (a) displays the standard layout of the human aorta. (b) shows as typical configuration of an AD. Due to a primary entry tear on the inner vessel wall, blood flows through an additional channel in the aortic wall, referred to as FL. The main channel, where blood is still able to flow, is referred to as TL, as demonstrated in (c). The Stanford classification, as shown in (d), distinguishes between type A or type B aortic dissections. (e) shows an exemplar BAD.*

to one third, with BADs experience severe **complications** later in life [GGB*14, TvKJ*13]. In a significant proportion of patients (up to 50% in 5 years) the chronic FL continues to degenerate and grow in diameter over time, which increases the risk of fatal aortic rupture. The need for better risk stratification of patients with chronic AD has emerged in the last decade following the observation that early *thoracic endovascular aortic repair* (TEVAR) may potentially prevent late complications (after 5 years). Early identification of patients at high risk is thus highly desirable, because only high-risk patients would benefit from timely TEVAR. Patients at low risk for developing late complications would not benefit from TEVAR while being exposed to the small but significant procedural risk. Identifying specific morphologic features which might predict the risk of future adverse events has gained substantial research interest, since preemptive stent grafting might improve the long-term outcome of patients with BAD [NRE*09]. Several studies discovered that a large aortic diameter [GGB*14, TJvB*14, vBTR*14] and patient age of 66 years or more [GGB*14] seem to be associated with a higher risk for complications. Other studies have evaluated the growth rate of the diameter of the TL and FL as well [TvKJ*13].

In this work we aim to provide a framework for capturing and visualizing morphologic features of AD which can subsequently be used for assessing the risk of ADs in general, and BADs specifically. The contributions of this paper are:

- A visual baseline for assessing and comparing the risk of ADs by quantifying several features of the aorta.
- A visual *level-of-detail* (LoD) approach, offering physicians the possibility to analyze the influence of a specific feature at different granularities.
- Four different types of plots that are linked together and display various features: The diameter plot, the branching plot, the intervention plot and the event plot. Each of these shows the arrangement of a single feature, but can be combined together to assess the risk on a higher level.
- A novel composite visualization, referred to as *aortic dissection map* (ADM), the first visualization – to the best of our knowledge – that allows physicians to perform visual risk assessment of ADs based on several features simultaneously within a single view.

The paper is organized as follows: Section 2 reviews related work concerning visualization of risk predictions and glyph-based visualizations. Our contributions are described in Section 3. Details regarding the implementation are given in Section 4, and results are presented in Section 5. The paper is concluded in Section 6.

2. Related Work

As this paper utilizes techniques from various fields of visualization, we subsequently provide an overview of the most relevant work. Additionally, we describe how we utilize or adapt the presented methods in order to achieve our target objectives.

Diagnosis of Aortic Dissections. In clinical practice radiologists use CTA imaging for diagnosis and treatment planning of ADs [BNB*14]. Existing well-established approaches employ common medical visualization techniques to identify the spatial location and extent of possible ADs, and to judge on further treatment. New developments in the area of four-dimensional phase contrast magnetic resonance imaging will further improve the diagnostic process [CWG*12]. Our proposed ADMs provide means to visualize the diagnostic features identified by using imaging techniques.

Visualization of Risk. Risk in medicine can either mean the risk for developing diseases, or the risk for adverse events for diseased patients. The visual analysis of risk factors guides experts as well as patients to understand the effect of individual factors on the overall risk. In many cases visualizations make use of simple illustrations (e.g., bar or pie charts) to communicate information to a broad audience [LH99]. Zhang et al. [ZMN15] used color to depict the risk for cancer in human organs and other tissue. Born et al. [BSR*14] developed *Stent Maps* to visually convey predictions for adverse events in case of aortic implantations. Van Belle and Van Calster proposed visual cues for the visualization of risk prediction models in medicine [VBVC15]. Bögl et al. [BAF*14] implemented *TiMoVA-Predict*, a system for the analysis of temporal prediction models. For the visual representation of risk factors, Zolfaghar et al. [ZAS*13] proposed *Risk-O-Meter*, a system to calculate and visualize clinical risk factors. Our approach for visualizing the risk of adverse events follows the idea of *Risk-O-Meter*. In addition, we also include information about the spatial distribution of the features along the aorta,

and use more elaborate glyph-based techniques to communicate these information.

Glyph-based Visualization. Specific data attributes can be visually conveyed by glyphs. Borgo et al. [BKC*13] provided a comprehensive overview of glyph-based visualization in general. By considering aspects of semiotics, glyphs can exhibit different comprehension time. Guidelines for applying glyphs in medical visualizations are presented by Ropinski et al. [ROP11]. They use superquadric glyphs mapped to surfaces such as the skull or heart. Mlejnek et al. [MEVB*05] present *profile flag*, a composite glyph for analyzing the cartilage of the knee within T_2-weighted *magnetic resonance imaging* (MRI) data sets and its extension for assessing the temporal development of breast-cancer lesions in *dynamic contrast-enhanced MRI* (DCE-MRI) data sets [MEVB*06]. Straka et al. [SCC*04] present *VesselGlyph*, an approach to combine a specialized visualization of a vessel lumen (*focus*) with a visualization of the vessel's surroundings (*context*). We use composite glyphs to provide a concise overview of different aspects of ADs.

3. Methodology

We postulate that the future risk of a patient can be quantitatively assessed by combining different features of the diseased aorta. First, we inspect the largest aortic diameter, because it is a known risk factor and expected to increase over time in ADs (cf. Section 3.1). The second feature we capture is the outflow of blood from the aortic TL and FL through the respective branch vessels (cf. Section 3.2). The more patent branch vessels arise off and thus drain the FL, the lower the risk of aneurysmal dilatation over time – presumably due to lowering the diastolic pressure. The third feature is the number and type of interventions performed in a patient, as the type and extent of intervention likely modifies the future risk (cf. Section 3.3). The last assessed feature is the aggregate probability of adverse event-free survival for one, two and five years after the initial hospitalization (cf. Section 3.4).

The current clinical workflow and our proposed extended solution are illustrated in Figure 2. At most institutions the current standard of care in reporting aortic dimensions in clinical practice is typically a narrative description of imaging findings, which includes the maximum diameter measured at time of interpretation by the radiologist. At our institution, which is an academic aortic center, aortic diameters are routinely measured manually by dedicated 3D-technologists, following a standardized protocol for every patient with AD. The measurements are obtained at baseline, and at every follow-up, typically obtained at 3, 6, and 12 months (and annually thereafter). The diameter measurements supplement the radiology report as a simple table pasted into the radiology report from the database containing the measurements. Currently, no commercial tool is available supporting the visual analysis of key anatomic features, and allowing to compare and combine them between patients and within patients over time. Additional features, such as branch vessel outflow, and other possible candidate features for predicting adverse events are currently captured for investigational purposes only. We therefore explicitly decided to create a flexible visualization technique, that allows radiologists to capture and analyze a broad variety of different features. With our proposed ADMs it is very easy to use the features for further analysis (e.g., new risk calculations) or to include findings (e.g., new interesting features) in the visualization. Our solution complements the current workflow, but could ultimately be included in the routine workflow. The feature visualization can be translated easily. Once the results of the risk models, which are based on the captured data, are sufficiently validated, those can be translated for routine use as a treatment decision aid in the future as well.

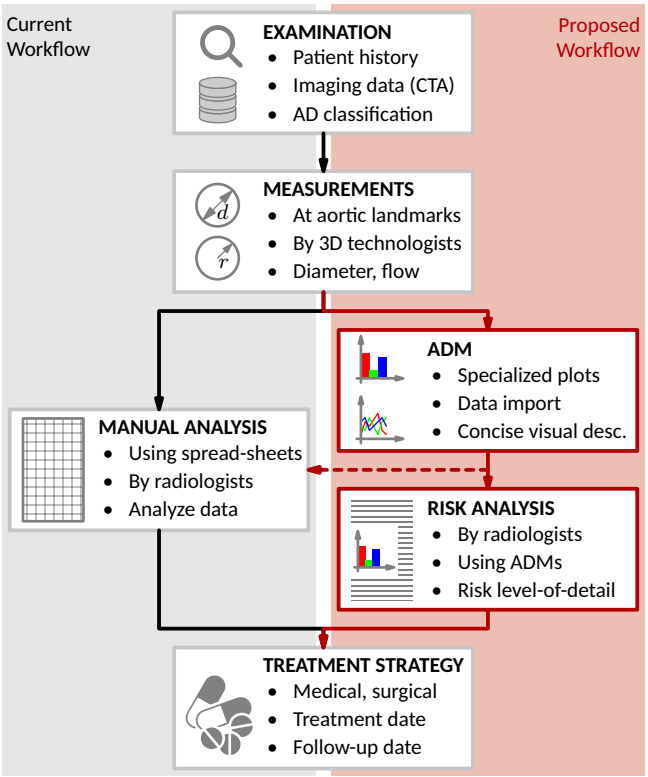

Figure 2: *Treatment procedure of ADs. After imaging data are acquired, aortic features (diameter, flow) are measured by 3D technologists at specific landmarks along the aorta. In the current workflow (left side) these features are subsequently inspected using spreadsheets (Excel) to derive a proper treatment strategy. Our proposed workflow (right side) imports the measurement data and automatically generates a report that consists of specialized plots. These plots can complement the current workflow or enable a thorough risk analysis to make an optimized treatment decision.*

The features which are analyzed in our plots are measured at certain positions along the aorta. Eleven landmarks, L_i, have been defined according to their positions along the aorta (cf. Figure 1a). The positions of the landmarks in our plots correspond to the averages of the respective landmark positions in a typical dissection population. We use the landmarks as spatial reference points in our plots. The landmarks are the following, with their distances from the beginning of the aorta given in brackets: *1)* Ann (0 cm), *2)* SOV (1.414 cm), *3)* STJ (2.722 cm), *4)* MidAsc (6.154 cm), *5)* Parc (9.586 cm), *6)* Darc (13.76 cm), *7)* Pdes (19.88 cm), *8)* Ddes (29.94 cm), *9)* Celiac (40.72 cm), *10)* Renal (45.54 cm), and *11)* Bif (55.74 cm). The aorta is further divided into the following five seg-

ments, each spanning over specific landmarks: *1)* the aortic root (L_1 to L_3), *2)* the ascending aorta (L_4), *3)* the aortic arch (L_5 and L_6), *4)* the descending thoracic aorta (L_7 and L_8), and *5)* the abdominal aorta (L_9 to L_{11}). This subdivision of the aorta is used throughout this work for measurements of several features.

The measured features are visualized in our proposed glyph-based visualization, called *aortic dissection map* (ADM), which consists of several specialized plots. In order to visually convey the risk of a specific feature, we chose a diverging color map from green over yellow to red, with red being severe. The same color map is used throughout all our proposed plots and has been chosen according to the suggestions for diverging color maps for scientific visualization by Morelend [Mor09]. All the plots presenting various features are combined to form a concise overview of the current state of the aorta. In this combination, the information can be accessed at different LoDs, which are described in Section 3.5 in detail. As an important part, we provide an *aggregated risk* value for every plot.

3.1. Diameter Plot

ADs result in an enlargement of the aorta. The aortic diameters are currently measured manually by 3D technologists at specific landmarks along the aorta (cf. Figure 1a). The major and minor aortic diameters are determined by aligning an oblique slice plane at the landmarks' positions on the aortic centerline and gathering them by placing a ruler. Despite measuring the minor diameter, only the major is of clinical interest at the moment. An example diameter plot is presented in Figure 3, showing the average landmark positions along the aorta on the left, the aortic segments on the right in blue and the measured major diameters in centimeter. The x-axis shows the major diameter in centimeters, and the y-axis acts as the symmetry axis of the aorta. We specifically developed this design with our domain experts to reflect the shape of the aorta.

The major aortic diameter typically grows over time, likely a result of a mismatch of tensile strength of the dilating aortic wall and luminal pressure. A large diameter indicates an advanced state of AD and once the risk of rupture exceeds the risk of surgical morbidity and mortality, surgical repair is indicated. A healthy diameter, d_{healthy}, defaults to three centimeters. The *soft limit*, d_{soft}, is usually around 5 cm and the *hard limit*, d_{hard}, around 6 cm. Exceeding d_{soft} acts as a warning and should alert radiologists to prepare for upcoming interventions, or to schedule an examination immediately or in the near future. Having a major diameter larger than d_{hard} is considered critical and requires immediate care.

Other influential factors are genetic disorders, such as a connective tissue disease (e.g., *Marfan syndrome*). In those cases, both diameter limits are reduced by one centimeter and adverse events are more likely to appear. Motivated by the work of Kim et al. [KCH10] and Waser et al. [WFR*10] we visualize dissections as lines branching off the centerline of the aorta. ADs have a begin and an end together with the location of the primary entry tear along the path. The tear does not necessarily coincide with the beginning of the AD, since blood may also flow retrograde when entering the media layer of the aortic wall.

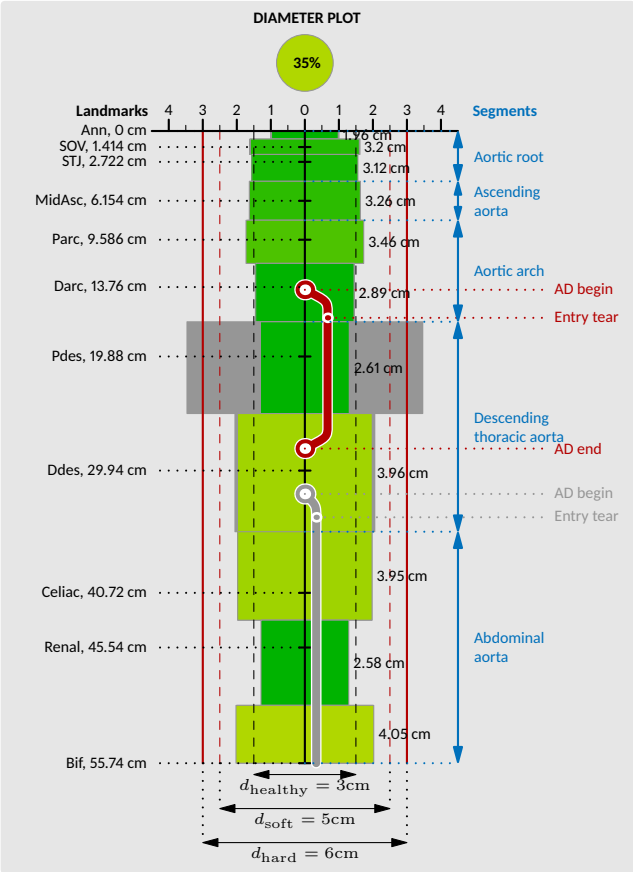

Figure 3: *Diameter Plot. The y-axis displays the aorta in a straightened fashion with the ticks representing the eleven aortic landmarks. Since these landmarks are not evenly spaced, we show their average distances on the left side in black. The x-axis is symmetric around the y-axis showing the aortic diameter. The aortic segments are shown on the right in blue. Two ADs are shown, one in red and another one in gray. The former one, a FL, contains a begin, entry tear and an end of the dissection. The gray dissection is thrombosed and has a begin, an entry tear, but no end within the aorta. The aggregated risk is shown on top of the diameter plot.*

In our divergent color map, the major diameter is mapped with d_{healthy} to green, over yellow, to d_{hard} being red. This allows physicians to quickly identify critical regions along the aorta. The aggregated risk of the diameter plot, $\mathcal{R}_{\text{DP}}$, is estimated as the largest of the major diameters of all landmarks:

$$\mathcal{R}_{\text{DP}} = \max_{\forall l \in L}\left(\frac{\min(\max(d(l), d_{\text{healthy}}), d_{\text{hard}}) - d_{\text{healthy}}}{d_{\text{hard}} - d_{\text{healthy}}}\right), \quad (1)$$

where $d(l)$ is the major diameter at landmark l. The risk is normalized between zero (d_{healthy}) and one (d_{hard}), where a higher value indicates higher risk, as the largest diameter tends to approach or even exceed d_{hard}. In such a case, other features might be useful to consider, since, especially for BADs, surgical treatment might not be immediately recommended.

3.2. Branching Plot

The branching plot (cf. Figure 4) presents the blood outflow volume of all 21 arteries connected to the aorta. The first branches are the coronary arteries left and right (CAL and CAR) of the aortic root segment, followed by the ascending aorta without branches, visually conveyed by the empty region in the plot. The aortic arch has three outgoing arteries (AA1–3), the brachiocephalic trunk, the left common carotid artery and the left subclavian artery. The descending thoracic aortic segment consists of 16 outbound intercostal arteries (IA1–16). The last segment, the abdominal aorta, branches to the celiac artery (CEA), the superior mesenteric artery (SMA), the renal arteries left (RAL) and right (RAR), the inferior mesenteric artery (IMA) and the iliac arteries left (ILAL) and right (ILAR).

Drainage of the FL outflow is estimated as the sum of blood supplied to each branch artery arising off the FL. The flow rates for the left subclavian artery (275mL/min), the celiac (550mL/min), superior (550mL/min) and inferior (190mL/min) mesenteric arteries, the renal arteries (500ml/min each) and the iliac arteries (400mL/min each) are based on reference data for resting blood flow in humans with a cardiac output of 7 liters per minute [WL89]. If a vessel originates from both channels, the flow is equally split between the TL and FL, respectively. The higher the FL outflow, the better, presumably because better drainage of the FL reduces the diastolic pressure, and thus the FL wall tension. If an outbound artery is connected to the TL or FL, it is shown by the letters *T* or *F* within the respective artery box. As obtained by experiments of our domain experts, only the number of present intercostal arteries is relevant, regardless their connected lumen [FMM08].

The blood outflow is color-coded in red for high risk (zero outflow), over yellow, to green for low risk (high outflow). Since blocked arteries are displayed with empty boxes in the plot and their outflow would not be visible, we show them by coloring their names according to their outgoing flow percentage. The aggregated risk of the branching plot is assumed to increase with decreasing overall outbound blood volume. Therefore, we estimate the aggregated risk for the branching plot as one minus the average outflow:

$$\mathcal{R}_{\mathrm{BP}} = 1 - \frac{1}{|B|} \cdot \sum_{i=1}^{|B|} vol(B_i) \qquad (2)$$

with $vol(B_i)$ being the blood outflow volume of outbound artery branch B_i. Again, the risk is normalized between zero and one. Risky regions are initially treated medically, but with advancing risk they have to undergo surgical revascularization.

3.3. Intervention Plot

The intervention plot (cf. Figure 5) displays all surgical interventions during the course of the AD disease of a single patient. It is vital to track the intervention history of patients to plan upcoming therapeutic treatment options or, combined with the diameter plot, examine the major diameter decrease after an intervention. Two different types of revascularization are currently employed to restore the blood flow channel.

The first option is placing an *endograft* to cover the primary entry tear and restore aortic blood flow to the TL. Endografts are

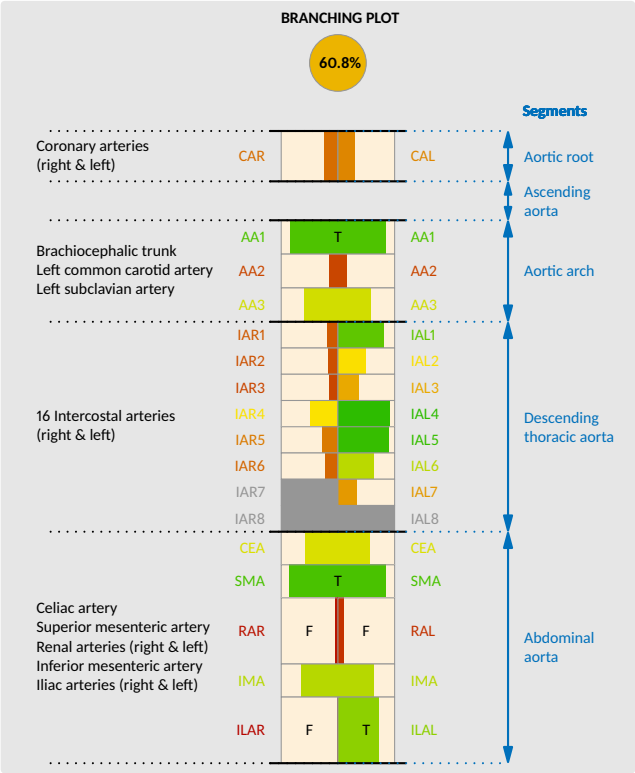

Figure 4: *Branching Plot. All arteries (in black on the left side) connected to the aorta are shown, subdivided according to the aortic segments (in blue on the right side). For each artery, the outgoing blood flow volume is displayed and if measured, the connected lumen is also shown (either TL or FL) within the artery. Since a high outbound blood flow is considered healthy, the risk increases with less volume. The aggregated risk is shown on top of the plot.*

used to treat BADs and typically placed from the aortic arch into the descending aorta. The procedure is performed by inserting a catheter (endovascular intervention) through a groin artery with a wired stent (cf. Figure 5, illustrated with a cross-hatched pattern) fixated on a balloon. When the balloon reaches the desired target location in the aorta, it is inflated to widen the flow channel and place the stent that ensures perfusion after removal of the catheter. Since no surgery is required, this procedure is considered less invasive.

The second and more invasive procedure is open surgical repair with a synthetic *graft* to replace a portion of the aorta. Surgical repair is the treatment of choice for patients with AADs. A graft (cf. Figure 5, illustrated with a horizontal line pattern) is typically placed from just above the aortic root to the distal ascending aorta, but may extend further if required. Surgical grafts are made of woven or knitted Dacron or Gore-Tex.

Every intervention is associated with a certain risk. Hence, the aggregated risk of this plot is simply defined as the sum of all interventions, with a higher number representing higher risk:

$$\mathcal{R}_{\mathrm{IP}} = |I|, \qquad (3)$$

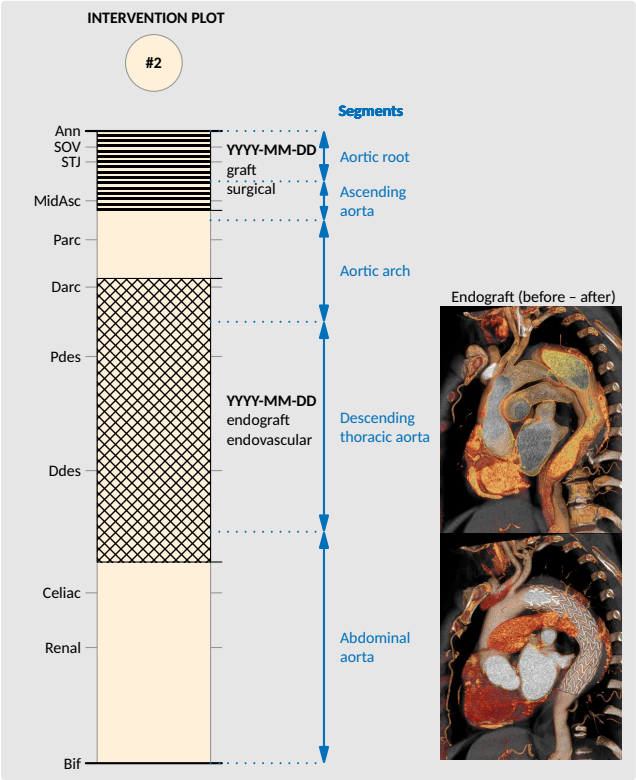

Figure 5: *Intervention Plot. The landmarks are shown on the left side and the aortic segments on the right in blue. Endografts are displayed with a cross-hatched pattern representing a wired stent and grafts are shown with a horizontal line pattern. The aggregated risk is shown on top of the intervention plot. The images on the right show a AD on top and the result of an endograft below. It is clearly visible that blood does not flow through the FL anymore.*

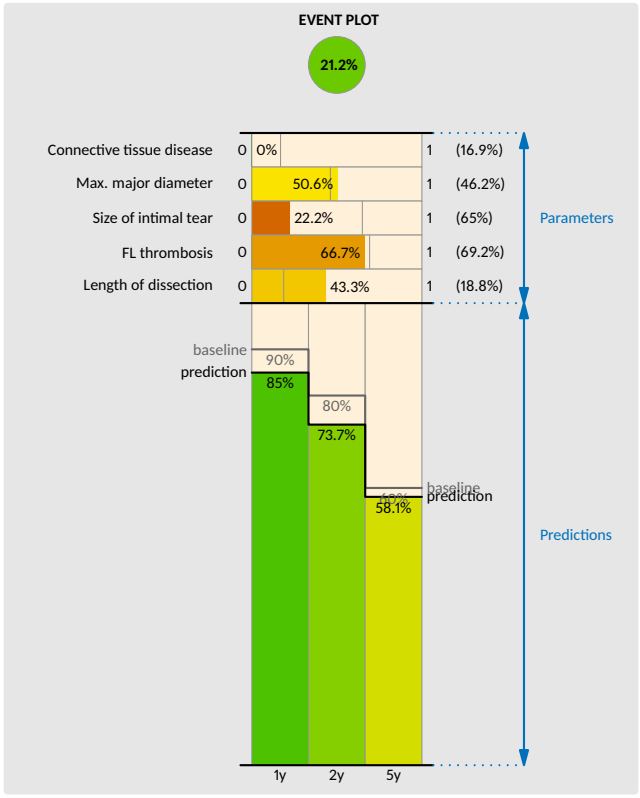

Figure 6: *Event Plot. The five parameters on top are the input of the prediction model. The adverse event-free probabilities are shown on the bottom with the three vertical bars representing the first, second and fifth year. The aggregated risk is shown on top of the plot.*

with I being the set of interventions. The effect of different surgical or endovascular procedures on late adverse events is not yet established. The purpose of this plot is to allow that this information is being captured to determine the respective effect on outcomes in single- and multivariate risk models in the future.

3.4. Event Plot

The event plot (cf. Figure 6) shows the probability to remain free of an adverse event for a time-frame of one year, two and five years. An adverse event is considered to be a surgical intervention such as endografting or stentgrafting, as reflected in the intervention plot. Motivated by the work of Grommes et al. [GGB*14], we designed a visualization that is based on five features as input parameters, and shows the adverse event-free probabilities below. The first and the most discriminative parameter is whether the patient suffers from a connective tissue disease, i.e., a genetic disorder such as the *Marfan syndrome*. This parameter can only be true (100%) or false (0%), and in the former case reduces the soft and hard limits of the diameter plot by 1 cm each. The second parameter is currently set to the maximum of the major aortic diameters. Its upper limit is eight centimeters, which is mapped to 100% risk. Since the influence of other features are currently unknown, but subject to investigations, we assigned the following three other parameters between zero and one: the size of the intimal tear, the FL thrombosis, and the length of the dissection. These parameters were selected according to the suggestions of our collaborators. We then empirically chose baseline probabilities for the upcoming years as 90%, 80% and 60%. This offers a comparison to a larger patient cohort. The adverse event-free probabilities are estimated as follows:

$$y(i) = 2 - \max(0.25, \overline{P})^{-1/W(i)}, \qquad \forall i \in \{1,2,5\} \tag{4}$$

with $W(1) = 5$, $W(2) = 3$ and $W(5) = 2$, weighting the first year most, the second less and the fifth least. $\overline{P}$ defines the average value of all five input parameters, with a value below 0.25 considered as severe, since it prognoses an adverse event with 100% in the upcoming five years. This prediction model was chosen to show the possibility of a visual representation of risk in our proposed plot. The risk values shown in this work are a best educated guess, based on current literature and our own clinical and research findings. We currently calculate risk for uncomplicated BADs, and provide it to the surgeons who have been involved in the research to establish that score, but it is not used for decision making.

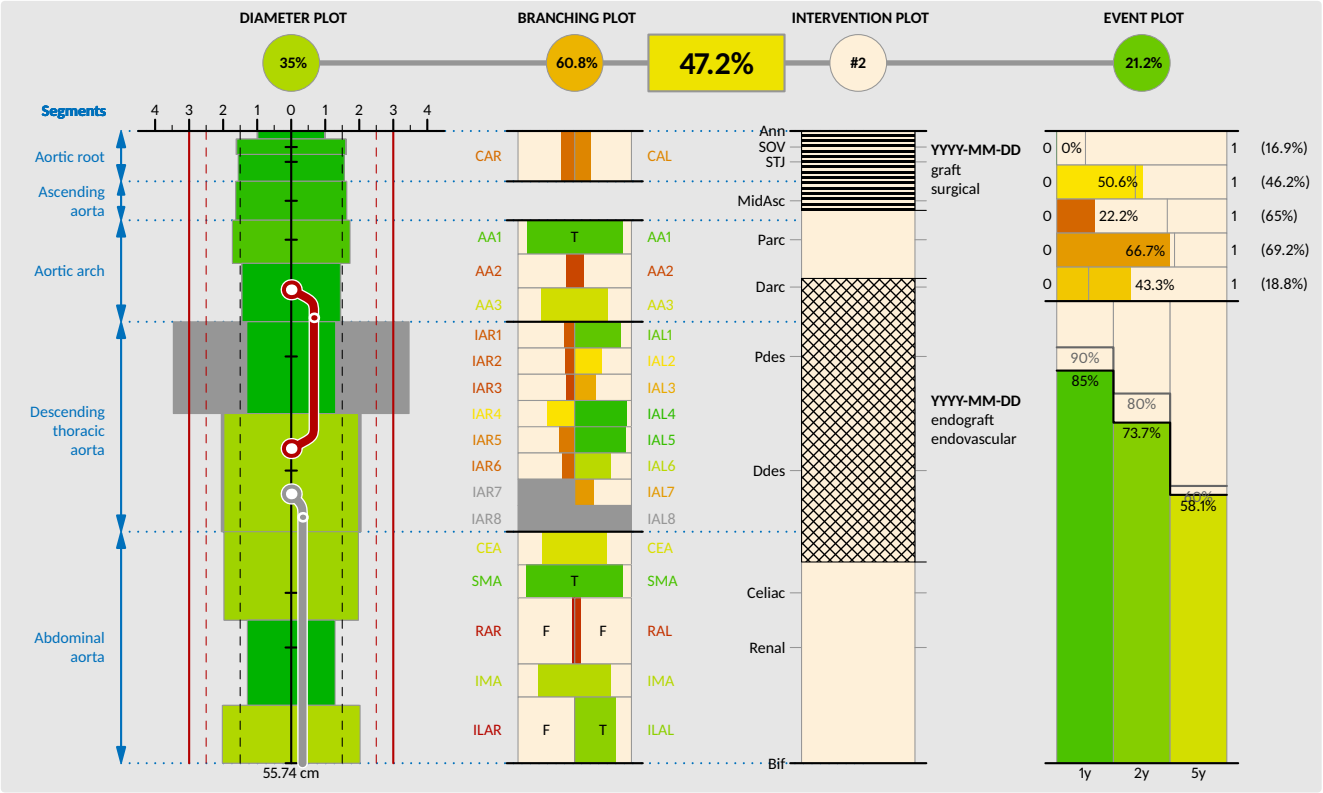

Figure 7: *Aortic Dissection Map. The map consists, from left to right, of a diameter plot, a branching plot, an intervention plot and an event plot. The aortic segments are linked within the first three plots, since they are not reflected in the event plot. The ADM exhibits three different risk LoDs. Starting with the coarsest level, the overall aggregated risk is shown in the box at the top-center. The next finer risk level are the aggregated risk values per plot, displayed in circles above each plot. The last and finest level are the plots themselves, because one can accurately identify which feature contributes to the current risk value.*

The aim of this plot is to show the adverse event-free probability in the upcoming years. This helps to decide upon the treatment strategies, e.g., the time of follow-up examinations, or the type of possible interventions (medically or surgically). The aggregated risk of the event plot is estimated as:

$$\mathcal{R}_{\text{EP}} = 1 - \frac{1}{8} \cdot (5y(1)) + 2y(2) + 1y(5)) \tag{5}$$

with $y(\cdot)$ being the adverse event-free probability of years in the future. As further predictions tend to be less accurate, the weighting decreases accordingly. There is no generally accepted risk model to prevent aortic aneurysm formation after AD. Before the advent of TEVAR, only the risk of rupture associated with aortic dilatation and aneurysm formation was clinically important. Once the risk of rupture, based on aneurysm diameter, exceeded the surgical risk, the indication for surgical repair was established. Under the current paradigm, the goal is to predict future risk and prevent aneurysm development by preemptive endografting.

3.5. Aortic Dissection Map (ADM)

The basic set of plots as described in the previous Sections, are combined into the *aortic dissection map* (ADM). With this composite visualization we propose the first visual tool to analyze and quantify ADs. The most important aspect is that the x-axis of an ADM can be seen as a timeline, since whenever new measurements are acquired, a corresponding plot can be added to the right of the existing ones. Plots can be added and removed, depending on their importance and need. This offers a very flexible design of inspecting a patient's history. New findings can be very easily integrated into the ADM. Figure 7 shows an exemplar ADM comprising one of the described plots each. All landmarks and segments are visually linked to preserve the context between the separate plots, motivated by the work of Steinberger et al. [SWS*11].

Since we compute an aggregated risk value for each plot separately, we add another LoD and estimate the overall aggregated risk of the ADM, the large box in the top-center of Figure 7, as follows:

$$\mathcal{R}_{\text{ADM}} = (\log_{10}(\max(\mathcal{R}_{\text{IP}}, 1) + 1) \cdot \frac{\mathcal{R}_{\text{DP}} + \mathcal{R}_{\text{BP}} + \mathcal{R}_{\text{EP}}}{3} \tag{6}$$

We assume that risk increases logarithmically with the number of interventions, modeled with the first factor. The second factor is the average of the risk factors of the other plots. Despite estimating the risk factors, the primary goal are the visual means to convey them. This visual representation of different risk LoDs allows the

physician to quickly identify possible sources of high risk following a top-down approach. At the top of the ADM, the most discriminating features can be identified. The individual plots can then be analyzed to get more information about the spatial location of the risky regions, or to analyze certain features in more detail.

4. Implementation

We explicitly chose LaTeX and Asymptote [BH08] to ensure proper integration into the clinical workflow (cf. Figure 2). All plots have been implemented in Asymptote and are embedded in LaTeX code. Whenever a report has to be generated, the required measurement data is exported to CSV files and passed to the generation script that forwards the respective parameters to the LaTeX code of the report. The measurements are then read in the Asymptote code of the corresponding plots. This process facilitates flexible input of the data without any adjustments and it extends the current clinical workflow with a minimum of necessary user interaction.

5. Results and Discussion

Several ADMs of different data sets are presented in this section. First, we present a phantom data set to illustrate the capabilities of our plots and the ADM. With the second and third data set, we present two current patient cases in order to highlight the contributions of our visualization techniques.

The ADM created with the exemplary phantom data set can be seen in Figure 7. The diameter plot is an exception in this data set, since it reflects real data. The patient had a severely enlarged aorta (gray area) in the descending thoracic segment and underwent revascularization by applying an endograft (green overlay). Although the adverse event-free probabilities are quite high, the outflow volume is generally very low and two interventions have taken place, leading to an aggregated risk of 47.2%. The ADM offers a LoD possibility by first checking the overall aggregated risk, then the individual ones of each plot and finally, every feature in detail. This allows physician to perform a thorough AD assessment.

Figure 8 demonstrates a stable patient with an AD. The aorta is quite dilated as shown by the yellow major diameters in the first three aortic segments. The dissection begins in the arch and ends in the abdominal aorta, and the branching plot indicates reduced outflow at the beginning of the dissection (cf. Figure 8a). As the adverse event-free predication is high, this patient is considered stable with an aggregated risk of 31%. The primary entry tear is highlighted with an orange arrow in the left image of Figure 8b, and the entire span of the dissection is visible in the right image. Figure 8c presents two sagittal views of the dissection onset. The ADM allows a comprehensive overview while retaining details of every inspected feature.

A patient with a fast progressive AD is shown in Figure 9. The diameter plot (cf. Figure 9a) presents the measurements of two investigations that have been 221 days apart. At the first one, the major diameter in the descending thoracic region exceeded the soft limit and therefore, an endograft was applied, as illustrated in the interventions plot, spanning the descending thoracic segment to the abdominal aorta. The endograft can be seen in the coronal view (cf. Figure 9b), together with the eliminated perfusion of the FL, as highlighted in the axial images (cf. Figure 9c) with the orange arrows. Reading the ADM, one can clearly follow the patient's history and understand why certain decisions have been made – one of the primary goals of our contribution.

Our proposed plots build on the basic principle to condense the represented information into a schematic form while preserving contextual anatomic information. The strength of the features predicting the risk of late adverse events is currently the subject of intense investigations. For patients with uncomplicated BADs, our collaborators have recently shown and quantified the association with diameter, circumferential extent of FL wall detachment, number of intercostal arteries arising off the dissected aorta, and FL outflow in a single aggregate risk score. For chronic AADs, the predictive power of these or other features have not been established. The present work will enable such investigations, because it provides the necessary framework to capture the plausible features in a systematic fashion, display them, and subject them to subsequent visual analysis.

The ADM has been informally presented to a panel of cardiothoracic surgeons and interventional radiologists at several occasions during interdisciplinary meetings. While it has not been presented to patients yet, similarly designed simple plots of diameters only are used on a regular basis at follow-up clinic visits at our institution. Our collaborators are convinced that with the ADM patients fully understand and see ADs for the first time. Several iterations through clinical studies will be required to determine a set of discriminative anatomic features, but for this purpose our ADMs act as a baseline.

6. Conclusions and Future Work

We presented a combination of glyph-based plots for describing different features of aortic dissections. These plots can either be used on their own to analyze the diameter, the blood outflow volume, interventions and the risk for adverse events separately, or in combination to get a concise overview of the current state of a patient's aorta. A LoD approach allows physicians to immediately recognize critical features. Our proposed visualization forms a baseline comparison for the analysis of risk parameters in case of ADs.

One interesting future aspect is comparing several different risk models with more parameters in the ADM. Although we are already working on a *risk calculator* which interactively updates the risk estimate when changing the input parameters for a hypothetical patient, we felt this is too premature to include in the present manuscript. Hence, current reports are static, but will be extended with interaction capabilities in the future together with the possibility to analyze temporal changes of a single patient.

References

[BAF*14] Bögl M., Aigner W., Filzmoser P., Gschwandtner T., Lammarsch T., Miksch S., Rind A.: Visual Analytics Methods to Guide Diagnostics for Time Series Model Predictions. In *Proceedings of the 2014 IEEE VIS Workshop on Visualization for Predictive Analytics* (2014), Perer A., Bertini E., Maciejewski R., Sun J., (Eds.). 2

[BH08] Bowman J. C., Hammerlindl. A.: Asymptote: A vector graphics language. *TUGBOAT: The Communications of the TeX Users Group 29*, 2 (2008), 288–294. See also http://asymptote.sourceforge.net/. 8

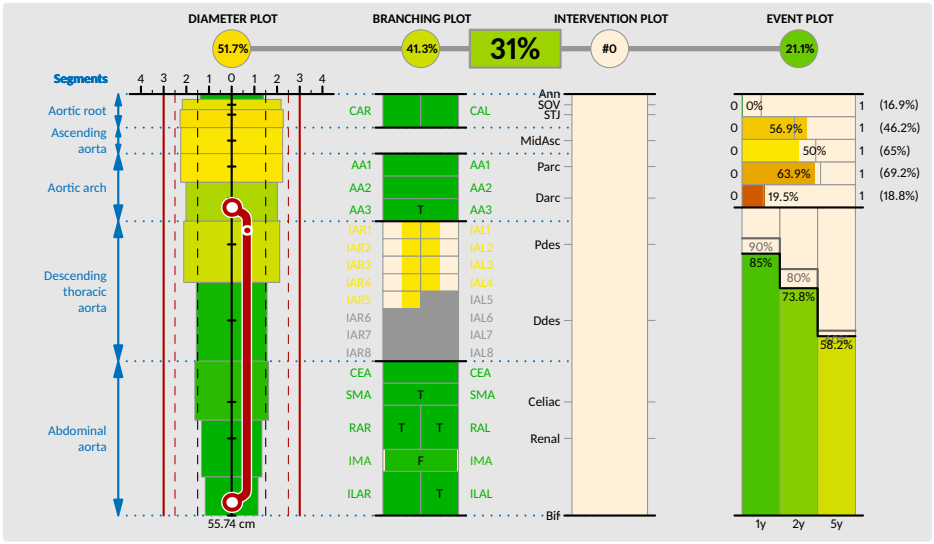

(a) ADM

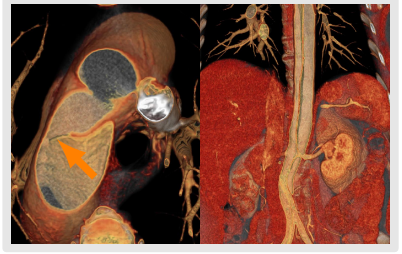

(b) Axial & Coronal Views

(c) Sagittal Slices

Figure 8: *Patient with a stable AD. The major aortic diameter is quite large until the descending thoracic aorta, as shown in (a). The dissection starts in the aortic arch – the primary entry tear is highlighted with a orange arrow in the left image of (b) – and lasts until the abdominal aorta, as shown in the right image of (b). The branching plot shows a decreased outflow from the beginning of the dissection. No interventions have taken place, since the patient is considered stable due to the low probability of adverse events in the upcoming years.*

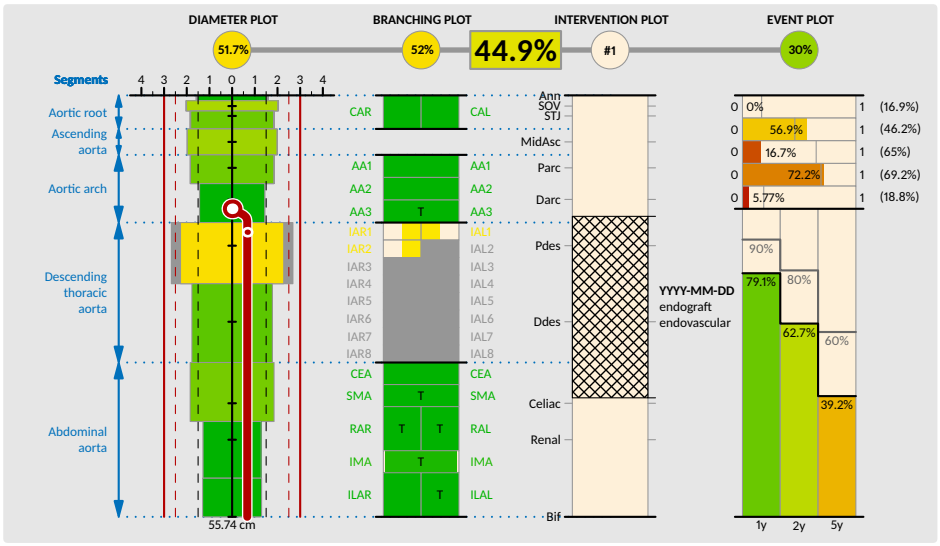

(a) ADM

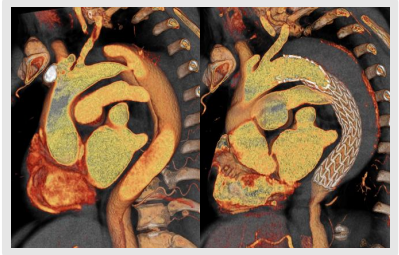

(b) Coronal Views

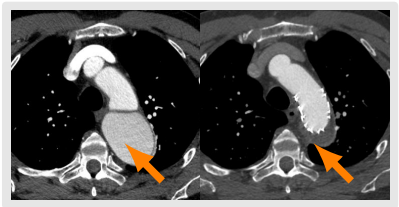

(c) Axial Slices

Figure 9: *Patient with fast progression of AD. The AD is shown in the diameter plot (a) with a large major diameter (gray) in the descending thoracic segment. The dissection does not have a defined end within the aorta and the entry tear is located in the critical region, as strengthened by the reduced outflow volume in the branching plot. After applying an endograft, as presented in the intervention plot, this particular diameter is reduced (yellow). This is also visible in the images on the right side, where (b) shows a coronal view with perfused FL on left and a thrombosed on the right after endograft deployment. (c) shows axial slices, again before and after the intervention. The aggregated risk is rather average and the risk of an adverse event in the upcoming years is 30%.*

[BKC*13] BORGO R., KEHRER J., CHUNG D. H., MAGUIRE E., LARAMEE R. S., HAUSER H., WARD M., CHEN M.: Glyph-based visualization: Foundations, design guidelines, techniques and applications. In *Proceedings of Eurographics State of the Art Reports* (2013), pp. 39–63. doi:10.2312/conf/EG2013/stars/039-063. 3

[BNB*14] BALIGA R. R., NIENABER C. A., BOSSONE E., OH J. K., ISSELBACHER E. M., SECHTEM U., FATTORI R., RAMAN S. V., EAGLE K. A.: The Role of Imaging in Aortic Dissection and Related Syndromes. *JACC: Cardiovascular Imaging 7*, 4 (2014), 406–424. doi:10.1016/j.jcmg.2013.10.015. 2

[BSR*14] BORN S., SÜNDERMANN S. H., RUSS C., HOPF R., RUIZ C. E., FALK V., GESSAT M.: Stent Maps - Comparative Visualization for the Prediction of Adverse Events of Transcatheter Aortic Valve Implantations. *IEEE Transactions on Visualization and Computer Graphics 20*, 12 (2014), 2704–2713. doi:10.1109/TVCG.2014.2346459. 2

[CWG*12] CLOUGH R. E., WALTHAM M., GIESE D., TAYLOR P. R., SCHAEFFTER T.: A new imaging method for assessment of aortic dissection using four-dimensional phase contrast magnetic resonance imaging. *Journal of Vascular Surgery 55*, 4 (2012), 914–923. doi:10.1016/j.jvs.2011.11.005. 2

[DTS*70] DAILY P. O., TRUEBLOOD H. W., STINSON E. B., WUERFLEIN R. D., SHUMWAY N. E.: Management of acute aortic dissections. *Annals of Thoracic Surgery 10*, 3 (1970), 237–247. doi:10.1016/S0003-4975(10)65594-4. 1

[FMM08] FLEISCHMANN D., MITCHELL R. S., MILLER D. C.: Acute aortic syndromes: New insights from electrocardiographically gated computed tomography. *Seminars in Thoracic and Cardiovascular Surgery 20*, 4 (2008), 340–347. doi:10.1053/j.semtcvs.2008.11.011. 1, 5

[GGB*14] GROMMES J., GREINER A., BENDERMACHER B., ERLMEIER M., FRECH A., BELAU P., KENNES L. N., FRAEDRICH G., SCHURINK G. W., JACOBS M. J., KLOCKER J.: Risk factors for mortality and failure of conservative treatment after aortic type B dissection. *Journal of Thoracic and Cardiovascular Surgery 148*, 5 (2014), 2155–2160. doi:10.1016/j.jtcvs.2014.03.053. 2, 6

[HBB*10] HIRATZKA L. F., BAKRIS G. L., BECKMAN J. A., BERSIN R. M., CARR V. F., JR D. E. C., EAGLE K. A., HERMANN L. K., ISSELBACHER E. M., KAZEROONI E. A., KOUCHOUKOS N. T., LYTLE B. W., MILEWICZ D. M., REICH D. L., SEN S., SHINN J. A., SVENSSON L. G., WILLIAMS D. M.: ACCF/AHA/AATS/ACR/ASA/SCA/SCAI/SIR/STS/SVM guidelines for the diagnosis and management of patients with thoracic aortic disease: A report of the american college of cardiology foundation/american heart association task force on practice guidelines, american association for thoracic surgery, american college of radiology, american stroke association, society of cardiovascular anesthesiologists, society for cardiovascular angiography and interventions, society of interventional radiology, society of thoracic surgeons, and society for vascular medicine. *Circulation 121*, 13 (2010), 266–369. doi:10.1161/CIR.0b013e3181d4739e. 1

[HBF*13] HOWARD D. P., BANERJEE A., FAIRHEAD J. F., PERKINS J., SILVER L. E., ROTHWELL P. M.: Population-based study of incidence and outcome of acute aortic dissection and premorbid risk factor control: 10-year results from the oxford vascular study. *Circulation 127*, 20 (2013), 2031–2037. doi:10.1161/circulationaha.112.000483. 1

[KCH10] KIM N. W., CARD S. K., HEER J.: Tracing genealogical data with timenets. In *Proceedings of Advanced Visual Interfaces* (2010), pp. 241–248. 4

[LH99] LIPKUS I. M., HOLLANDS J. G.: The visual communication of risk. *JNCI Monographs 25*, 25 (1999), 149–63. 2

[MEVB*05] MLEJNEK M., ERMES P., VILANOVA-BARTROLÍ A., VAN DER RIJT R., VAN DEN BOSCH H., GERRITSEN F. A., GRÖLLER M. E.: Profile flags: a novel metaphor for probing of T2 maps. In *Proceedings of the IEEE Visualization Conference* (2005), pp. 599–606. doi:10.1109/VISUAL.2005.1532847. 3

[MEVB*06] MLEJNEK M., ERMES P., VILANOVA-BARTROLÍ A., VAN DER RIJT R., VAN DEN BOSCH H., GERRITSEN F. A., GRÖLLER M. E.: Application-oriented extensions of profile flags. In *Proceedings of the Joint Eurographics – IEEE VGTC Symposium on Visualization* (2006), pp. 339–346. doi:10.2312/VisSym/EuroVis06/339-346. 3

[Mor09] MORELAND K.: Diverging color maps for scientific visualization. In *Proceedings of the 5th International Symposium on Advances in Visual Computing, Part II* (Berlin, Heidelberg, 2009), ISVC '09, Springer Berlin Heidelberg, pp. 92–103. doi:10.1007/978-3-642-10520-3_9. 4

[NRE*09] NIENABER C. A., ROUSSEAU H., EGGEBRECHT H., KISCHE S., FATTORI R., REHDERS T. C., KUNDT G., SCHEINERT D., CZERNY M., KLEINFELDT T., ZIPFEL B., LABROUSSE L., INCE H.: Randomized comparison of strategies for type b aortic dissection: The INvestigation of STEnt grafts in Aortic Dissection (instead) trial. *Circulation 25*, 120 (2009), 2519–2528. doi:10.1161/CIRCULATIONAHA.109.886408. 2

[ROP11] ROPINSKI T., OELTZE S., PREIM B.: Survey of glyph-based visualization techniques for spatial multivariate medical data. *Computers & Graphics 35*, 2 (2011), 392–401. doi:10.1016/j.cag.2011.01.011. 3

[SCC*04] STRAKA M., CERVENANSKY M., CRUZ A. L., KÖCHL A., SRAMEK M., GRÖLLER E., FLEISCHMANN D.: The VesselGlyph: Focus & Context Visualization in CT-Angiography. In *Proceedings of IEEE Visualization* (2004), pp. 385–392. doi:10.1109/VISUAL.2004.104. 3

[SWS*11] STEINBERGER M., WALDNER M., STREIT M., LEX A., SCHMALSTIEG D.: Context-preserving visual links. *IEEE Transactions on Visualization and Computer Graphics 17*, 12 (2011), 2249–2258. doi:10.1109/TVCG.2011.183. 7

[TJvB*14] TRIMARCHI S., JONKER F., VAN BOGERIJEN G., TOLENAAR J., MOLL F., CZERNY M., PATEL H.: Predicting aortic enlargement in type B aortic dissection. *Annals of Cardiothoracic Surgery 3*, 3 (2014), 285–291. doi:10.3978/j.issn.2225-319X.2014.05.01. 2

[TvKJ*13] TOLENAAR J. L., VAN KEULEN J. W., JONKER F. H. W., VAN HERWAARDEN J. A., VERHAGEN H. J., MOLL F. L., MUHS B. E., TRIMARCHI S.: Morphologic predictors of aortic dilatation in type B aortic dissection. *Journal of Vascular Surgery 58*, 5 (2013), 1220–1225. doi:10.1016/j.jvs.2013.05.031. 2

[vBTR*14] VAN BOGERIJEN G. H. W., TOLENAAR J. L., RAMPOLDI V., MOLL F. L., VAN HERWAARDEN J. A., JONKER F. H. W., EAGLE K. A., TRIMARCHI S.: Predictors of aortic growth in uncomplicated type b aortic dissection. *Journal of Vascular Surgery 59*, 4 (2014), 1134–1143. doi:10.1016/j.jvs.2014.01.042. 2

[VBVC15] VAN BELLE V., VAN CALSTER B.: Visualizing Risk Prediction Models. *PLoS ONE 10*, 7 (07 2015), 1–16. doi:10.1371/journal.pone.0132614. 2

[WFR*10] WASER J., FUCHS R., RIBICIC H., SCHINDLER B., BLOSCHL G., GRÖLLER E.: World lines. *IEEE Transactions on Visualization and Computer Graphics 16*, 6 (2010), 1458–1467. doi:10.1109/TVCG.2010.223. 4

[WL89] WILLIAMS L., LEGGETT R.: Reference values for resting blood flow to organs of man. *Clinical Physics and Physiological Measurement 10*, 3 (1989), 187. 5

[ZAS*13] ZOLFAGHAR K., AGARWAL J., SISTLA D., CHIN S.-C., BASU ROY S., VERBIEST N.: Risk-O-Meter: An Intelligent Clinical Risk Calculator. In *Proceedings of the 19th ACM SIGKDD International Conference on Knowledge Discovery and Data Mining* (2013), pp. 1518–1521. doi:10.1145/2487575.2487717. 2

[ZMN15] ZHANG R., MIRKOVIC D., NEWHAUSER W. D.: Visualization of risk of radiogenic second cancer in the organs and tissues of the human body. *Radiation Oncology 10*, 1 (2015), 1–9. doi:10.1186/s13014-015-0404-x. 2